Theor Chim Acta (1993) 85: 199–207

Theoretica Chimica Acta

Nonrigid large van der Waals molecules

Joshua Jortner[1], Narda Ben-Horin[1], and Daphna Scharf[2]

[1] School of Chemistry, Tel Aviv University, Ramat Aviv, Tel Aviv 69978, Israel

[2] Department of Chemistry, University of Pennsylvania, Philadelphia, PA 19104, USA

Received December 31, 1991/Accepted May 13, 1992

Summary. We address the breakdown of the (nearly) rigid molecule description of molecular structure and spectra, which is realized when the amplitude of atomic motion becomes comparable with the average bond length. This situation prevails for van der Waals molecules and clusters at finite temperatures. Molecular nonrigidity was characterized in terms of an "intramolecular melting" Lindemann criterion, which reveals that aromatic molecule (M)–rare gas ($A \equiv Ar, Kr, Xe$) van der Waals molecules (clusters) are nonrigid at $T \geqslant 10$ K. A quantification of the concept of molecular nonrigidity in these systems was provided by constant energy molecular dynamics simulations for the smallest cluster of the $M \cdot A_n$ family, i.e., the one-sided $(2 \mid 0)$ benzene $\cdot Ar_2$ molecule, which reveals a hierarchy of isomerization phenomena with increasing temperature.

Key words: Van der Waals molecules – Nonrigidity – "Intramolecular melting" Lindemann criterion

1 Introduction

The traditional description of molecular structure implicitly relied on the notion of rigidity of each molecular species for its stereochemistry and chemical identification. In particular, the concept of chemical isomers rests on the rigidity of molecular structure, where the chemist interrogates different compounds having the same composition but distinct properties, including those observables (in particular, various methods of diffraction) from which we infer structures. As is well known, the assignment of chemical structures, i.e., the identification of physically and chemically distinguishable sites for an atom of a single kind within the molecule, is not isomorphous with the definition of a stationary molecular state in terms of permutation symmetry [1, 2]. The notion of molecular rigidity provided the cornerstone for molecular spectroscopy, which usually envisions nearly rigid molecular systems undergoing small-amplitude vibrations and overall rotations of the equilibrium structure. Of course, spectroscopic and molecular probing unveiled the limitations of the concept of molecular rigidity, as became first apparent from the inversion spectra of ammonia [3, 4]. Another

breakdown of rigidity involves the phenomenon of large amplitude concerted motion, i.e., pseudorotation in cyclopentane [5], phosphorous pentafluoride [1, 6] and bullvalence [7], which was originally advanced for nuclei [8]. Large-amplitude intramolecular motion was documented in several cases, e.g., with increasing size we would mention triatomic alkali molecules [9], which violate the small-amplitude vibrator model even in their ground state, the XeF_6 molecule [10], which exhibits large-amplitude internal motion spanning several local minima, and organometallic molecules, which undergo large-amplitude intramolecular rearrangements [11]. These fascinating deviations from molecular rigidity can be traced essentially to the existence of multiple minima in the molecular potential surfaces. In the realm of molecular chemistry and physics, these are exceptions which prove the rule.

The traditional rigid molecule picture breaks down when the amplitude of the intramolecular atomic motion becomes comparable to the average bond length (or to the size of the molecule). From the point of view of the spectroscopist very strong centrifugal and Coriolis coupling will prohibit the separation of rotation and vibration motion. Such a situation is realized for van der Waals molecules at finite temperature, spanning a broad range of molecular size from diatom-atom [12] up to aromatic molecules bound to rare gas atoms [13–17]. The strength of the van der Waals bond in such systems varies from $D \simeq 10\ \mathrm{cm}^{-1}$ for the $He-I_2$ [12] up to $D \simeq 350\ \mathrm{cm}^{-1}$ for benzene·Ar [15]. While at 0 K many of these systems are rigid, it is easy to accomplish the situation of excessive thermal excitation at a finite, relatively low temperature, whereupon extreme nonrigidity will be realized. The issue of nonrigidity of large van der Waals (vdW) molecules and clusters consisting of a large organic aromatic molecule bound to rare gas atoms (or to other ligands) [13–17], which is the subject matter of this paper, is of considerable intrinsic interest for the elucidation of the breakdown of the molecular rigidity concept. This phenomenon of the breakdown of cluster rigidity is expected to be size-invariant, being exhibited for both small and large clusters.

2 Characterization of nonrigidity

Correlation diagrams connecting the rotational energy levels of rigid and nonrigid three- and four-body molecular systems led Berry and his colleagues to advance a quantification of nonrigidity in terms of the ratio between the rotational and vibrational energy levels [18]. For larger systems a more general definition is required. In this context it will be useful to adopt some concepts which were utilized for the characterization of rigid-nonrigid transitions in clusters. A physical transparent approach can be based on the adaptation of the Lindemann melting criterion [19, 20], which rests on the notion of the onset of large-amplitude nuclear motion, whereupon the onset of nonrigidity is realized when the root mean square (rms) displacements of atom-atom distances normalized to the mean values exceed 10%–15%. For the sake of simple demonstration consider an idealized harmonic interatomic motion with a frequency ω and a reduced mass μ, with the zero-point rms displacement of $\delta_0 = (\hbar/\mu\omega)^{1/2}$. At a finite temperature T the rms displacement is:

$$\delta_T = \sum_v \exp(-v\hbar\omega/kT) v^{1/2} \delta_0 \Big/ \sum_v \exp(-v\hbar\omega/kT). \tag{1}$$

As the frequency ω is low for vdW molecules, the classical limit $kT > \hbar\omega$ can be realized, whereupon Eq. (1) reduces to:

$$\delta_T = \delta_0 (kT/\hbar\omega)^{1/2} \Gamma(3/2) \tag{2}$$

where Γ is the gamma function. The Lindemann criterion is:

$$\delta_T / \langle r \rangle \geqslant 0.1 \tag{3}$$

where $\langle r \rangle$ is the average interatomic distance. From Eqs. (2) and (3) we can define a rigidity parameter:

$$\varrho = (kT/\hbar\omega)^{1/2} (\delta_0 / \langle r \rangle) \tag{4}$$

and the nonrigidity condition is given by:

$$\varrho \geqslant 0.11. \tag{5}$$

Equation (5) can be viewed as an "intramolecular melting" Lindemann criterion. Let us apply Eq. (5) for large vdW molecules (which are often referred to as heteroclusters), consisting of an organic aromatic molecule (M) bound to rare gas (A ≡ Ar, Kr, Xe) atoms. For the parallel motion of the A atoms on the M surface the characteristic (anharmonic) frequencies are low, with typical values for Ar atoms being $\omega \sim 5\,\mathrm{cm}^{-1}$ [15], so that $\delta_0 \simeq 0.39$ Å and $\langle r \rangle \simeq 3.5$ Å [15]. The rigidity parameter at $T = 20$ K is $\varrho \simeq 0.20$, whereupon according to Eq. (5) these vdW molecules are nonrigid for the parallel motion of the rare gas atoms on the microsurface of M at this temperature. According to condition (5) the onset of nonrigidity in $M \cdot A_n$ molecules is expected to be exhibited at $T \gtrsim 10$ K. Of course, these arguments, which rest on the heuristic nonrigidity condition, Eq. (5), are qualitative. However, they are very useful and transparent for the elucidation of the interplay between the intrinsic molecular parameters and the external temperature in the characterization of the onset of molecular nonrigidity. Quantitative information regarding nonrigidity of these interesting large systems rests on quantitative molecular dynamics (MD) simulations. In what follows we shall present MD studies of rigid and nonrigid benzene·Ar_2 vdW heteroclusters, which constitute the smallest heteroclusters of the $M \cdot A_n$ family and which reveal a rich dynamic behavior.

3 Benzene·Ar_2 isomers

Benzene·Ar_2 heteroclusters are characterized by two isomers, the two-sided (1 | 1) structure, where a single Ar atom is located above each microsurface, and the one-sided (2 | 0) structure, with two Ar atoms located on one side of the microsurface. The spectroscopic studies of Schmidt, Mons and Le Calvé [21, 22] on the spectral shifts and rotational contours of the $S_0 \rightarrow S_1$ transition and the ionization potentials from S_0 for benzene·Ar_2 heteroclusters, provide compelling evidence for the existence of the (1 | 1) and the (2 | 0) isomers. Our MD simulations of the nuclear motion in S_0 of benzene·Ar_2 isomers, for which a preliminary report was previously presented [23], reval that: (i) The (1 | 1) structure constitutes a rigid molecule over a broad temperature domain, until it converts to the (2|0) structure at ~50 K. (ii) The (2 | 0) structure constitutes a nonrigid molecule over all the relevant temperature domains ($T \leqslant 70$ K), with an onset of isomerization processes at $T \geqslant 3$ K. (iii) The (2 | 0) benzene·Ar_2 heterocluster exhibits a hierarchy of isomerization processes with increasing temperature.

4 MD simulations

Classical MD simulations have been ubiquitous in the areas of molecular dynamics, condensed matter, cluster chemical physics and biophysics [24]. The validity conditions, which underline the applicability of MD simulations to the exploration of quantum systems by this purely classical approach, are well known [25] but rarely specified. The two validity conditions are:

(A) The localization condition. The thermal de Broglie wavelength of the particles $\lambda_T = \hbar/(\mu kT)^{1/2}$ (where μ is the effective mass) is considerably shorter than the characteristic lengths, e.g., the bond length $\langle r \rangle$, so that $\lambda_T/\langle r \rangle \ll 1$.

(B) The distinguishability condition. Permutation symmetry can be disregarded and distinguishability of identical particles can be realized provided that [25] $\exp[-(\langle r \rangle/\lambda_T)^2] \ll 1$.

Condition (A) is, of course, sufficient for the applicability of condition (B), whereupon only the former condition has to be considered. The localization condition can be expressed in the form $\hbar^2/\mu\langle r \rangle^2 \ll kT$. Alternatively, we can utilize the observables defined in Sect. 2 to recast condition (A) in the form:

$$(\delta_0/\langle r \rangle) \ll (kT/\hbar\omega)^{1/2}. \tag{6}$$

This validity condition for the applicability of classical MD should always be borne in mind. For van der Waals molecules, e.g., aromatic molecule-heavy rare gas heteroclusters (for which $\delta_0/\langle r \rangle \simeq 0.1-0.03$ and $\omega \simeq 5-40\ \mathrm{cm}^{-1}$ is low), we expect Eq. (6) to be well applicable over a broad temperature domain. For $M{\cdot}Ar_n$ clusters we expect that for $T \gg 0.2$ K the classical limit applies. Thus the validity conditions hold at low temperatures and classical MD can be applied with confidence to the problem at hand.

The constant energy MD simulations of benzene$\cdot Ar_2$ utilized a fifth-order predictor-corrector method for the integration of the equations of motion. The MD scheme was previously described [26]. The integration step was chosen as 10^{-15} sec at low temperatures ($T \leqslant 10$ K) and was gradually decreased with increasing temperature, being taken as 2×10^{-16} sec at $T \geqslant 60$ K. The first stage in the simulations involved an equilibration stage, with the initial random velocities being characterized by a Boltzmann distribution to give the desired temperature and with the total angular momentum being set to zero. A short simulation (10^5 integration steps) was then performed with the velocities being frequently scaled to achieve the desired temperature, followed by an uninterrupted short simulation to monitor the attainment of the final temperature. In some simulations we have used gradual heating of an equilibrated configuration for the initiation of the equilibrium stage. Subsequently, constant energy trajectories were generated in the ground electronic state for a time of 1.0–1.5 nsec. Energy was conserved in these simulations to better than 1 part in 10^7. The benzene molecule was taken to be rigid at its ground state equilibrium geometry. The potential surfaces of benzene$\cdot Ar_2$ heteroclusters in the ground electronic state were specified using Lennard–Jones atom-atom potentials [27]. The potential parameters for the C–Ar and H–Ar interactions were taken from the prescription of Ondrechen et al. [27]. Standard parameters were used for the Ar–Ar interaction. We tested the role of electrostatic benzene–Ar charge-induced dipole interactions within the ground state potential surface in order to ascertain their effects on the energetics and the relative stability of isomers.

Calculations of the charge-induced dipole interactions between the atomic charge distribution of benzene (obtained using the MNDO method [28] in conjunction with Löwdin's charge density analysis [29, 30]) and the rare-gas atom, resulted in the stabilization energy of $-6\ \mathrm{cm}^{-1}$ for the equilibrium nuclear configuration of benzene·Ar_1, which constitutes 1.5% of the total ground state binding energy, and can be safely neglected.

In each MD simulation the following observables were calculated by averaging over the entire trajectory: (i) The potential energy U. (ii) The standard deviation $\bar{\sigma}$ of the distances between the rare-gas atoms and the center of mass of benzene and the cartesian components $\bar{\sigma}_\xi$ ($\xi = x, y, z$) of $\bar{\sigma}$. The molecule fixed cartesian coordinate axes were specified by the origin at the center of mass of benzene, with x (in the molecular plane perpendicular to the C–C bond), y (in the molecular plane passing through two C atoms) and z (perpendicular to the molecular plane). We have also evaluated the normalized standard deviation σ, where the two contributions of the Ar atoms are normalized by their distances from the center of mass of benzene, and the normalized three cartesian components of σ, i.e., σ_x, σ_y and σ_z. (iii) The standard deviation δ of the Ar–Ar distance normalized by the average Ar-Ar distance. The MD simulations of the structure, energetics and nuclear dynamics of the $(1\,|\,1)$ and $(2\,|\,0)$ isomers of benzene·Ar_2 were performed over a broad temperature domain ($T = 3$–70 K). Static structural data were inferred from short time (100 psec) averaging of low-temperature ($T = 3$ K) simulations, yielding the equilibrium coordinates (x_1, y_1, z_1) and (x_2, y_2, z_2) of the two Ar atoms (in Å).

5 Dynamics of nuclear motion

From our MD simulations, the following information was obtained for the $(1\,|\,1)$ isomer:

(1) Its static low-temperature (3 K) equilibrium structure is (0, 0, 3.47) and (0, 0, −3.47), which corresponds to a D_{6h} symmetry.

(2) With increasing the temperature in the range 3–50 K, this structure (expressed by the average coordinates) is preserved.

(3) The potential energy U and the structural fluctuation parameters σ, σ_x, σ_y, σ_z and δ exhibit a smooth temperature dependence (Fig. 1). The increase of the structural parameters with increasing temperature is modest, e.g., σ increases from $\sigma = 0.005$ at 10 K to $\sigma = 0.06$ at 50 K.

(4) For $T \geqslant 52$ K the $(1\,|\,1)$ structure interconverts into the $(2\,|\,0)$ structure. This nearly irreversible $(1\,|\,1) \rightarrow (2\,|\,0)$ side crossing occurs already in the equilibration runs for the $(1\,|\,1)$ isomer.

Regarding the $(2\,|\,0)$ isomer we observed that:

(5) The low-temperature (3 K) static equilibrium structure is (3.24, 0, 3.13) and (−0.4, 0, 3.49), which reflects a low-symmetry (C_s) structure. One Ar atom is shifted (by 0.4 Å along the x axis) from the benzene·Ar minimum and the second Ar atom is located above the midpoint between two H atoms, with the Ar_2 dimer being slightly tilted relative to the benzene plane. Our structure of the $(2\,|\,0)$ isomer is in agreement with the recent results of Monte-Carlo simulations for this system [22]. This structure characterizes the heterocluster only at low

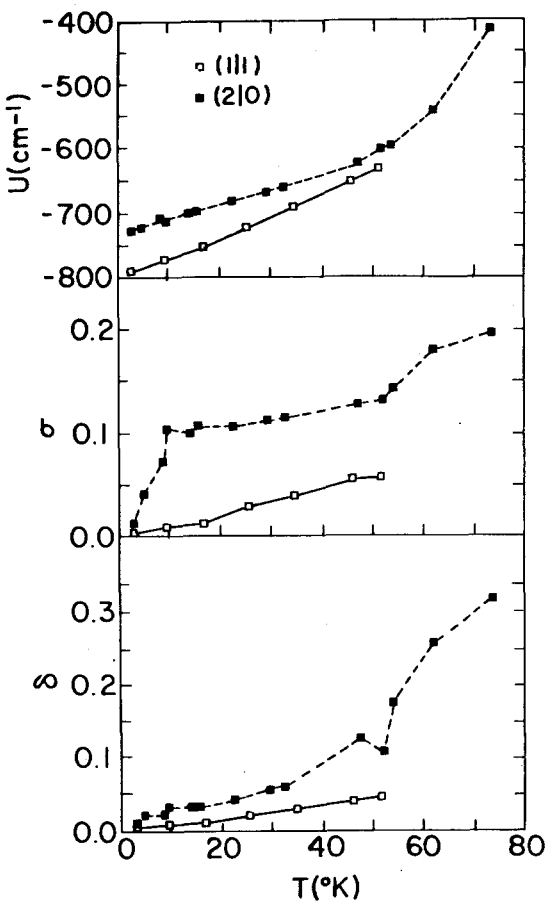

Fig. 1. The temperature dependence of the internal energy U and the normalized structural fluctuation parameters σ and δ for the (1 | 1) isomer (□) and for the (2 | 0) isomer (■) of benzene·Ar_2

temperatures, while at finite temperatures ($T \gtrsim 5$ K) large-amplitude motion sets in.

(6) The structural fluctuation parameters for the (2 | 0) isomer exhibit a non-smooth temperature dependence (Figs. 1 and 2), which marks the onset of a hierarchy of the following isomerization processes:
(a) Onset of correlated one-dimensional (1D) motion at $T \gtrsim 3$ K. The nuclear motion of the Ar_2 dimer along the x axis is enhanced with raising the temperature, as manifested by the rise of σ_x (Fig. 2).
(b) Onset of correlated 2D surface motion at 10 K. A steep rise in σ_y and a slight rise in σ_z are exhibited (Fig. 2), while σ_x and σ have already attained a high value (Figs. 1 and 2). Concurrently, δ does not reveal a break. These features mark the onset of a correlated 2D surface rotational motion of the Ar_2 dimer parallel to the benzene surface. These MD data concur with recent Monte-Carlo simulations, which reveal that the six equivalent H–C–C–H wells of the (2 | 0) isomer of benzene·Ar_2 are equally explored at 10 K [22].
(c) Onset of uncorrelated surface melting at 52–54 K. Here σ and δ exhibit a simultaneous increase of slope.

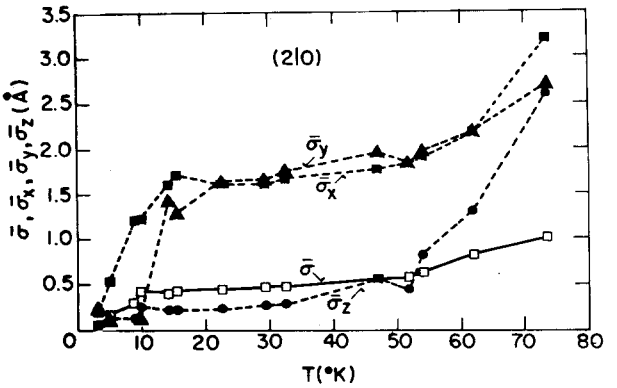

Fig. 2. The temperature dependence of the standard deviation $\bar{\sigma}$ (□) of the distances between the two Ar atoms and the center of mass of benzene and the cartesian components $\bar{\sigma}_x$ (■), $\bar{\sigma}_y$ (△), and $\bar{\sigma}_z$ (●) of $\bar{\sigma}$. Data for the (2 | 0) isomer of benzene·Ar_2

(d) Onset of side crossing at 47–54 K. Here σ_z exhibits a break followed by a sharp increase. The side crossing involves the motion of one Ar atom from (2 | 0) to the other side of the microsurface and back. The lifetime of the (1 | 1) structure is $\lesssim 5$ psec. The distinction between processes (c) and (d), which occur in the same temperature domain, was inferred from analysis of MD trajectories, which also sets the temperature limits for the onset of these isomerizations.
(e) Onset of 2D → 3D transition at 62 K. MD trajectories revealed the transition from the (2 | 0) structure to the $(1 + 1_2 \mid 0)$ structure, which contains one Ar atom in the first solvation layer ($z \simeq 3.5$ Å) and one Ar atom in the second solvation layer ($z \simeq 7.0$ Å). The lifetime of the 3D $(1 + 1_2 \mid 0)$ structure was 3–5 psec.

(7) At $T \geqslant 73$ K an efficient fragmentation process (2 | 0) → (1 | 0) + Ar sets in. Characteristic time scales for fragmentation of a single atom are ~300 psec at this temperature.

We are now in a position to compare the energetics and nuclear dynamics of the (1 | 1) and (2 | 0) isomers.

(8) The potential energy U of the (1 | 1) structure is lower than that of the (2 | 0) structure over the temperature range 3–52 K (Fig. 1). At the lowest temperature the (1 | 1) structure is energetically more stable than the (2 | 0) structure by $\Delta U = 55\ \mathrm{cm}^{-1}$, in accord with the estimate of Schmidt et al. [21], with the energy difference being reduced to $\Delta U = 10\ \mathrm{cm}^{-1}$ at 50 K. The energetic stability of (1 | 1) does not preclude the simultaneous formation of (1 | 1) and (2 | 0) isomers in supersonic expansions of Ar seeded with benzene [21].

(9) In the temperature range 3–52 K the (1 | 1) and (2 | 0) isomers do not interconvert on a time scale of 1 nsec.

(10) At temperatures above the onset of side crossing $T \geqslant 52$ K, the (2 | 0) structure is dominant. The dominance of the (2 | 0) structure at high temperatures is reflected by the nearly irreversible (1 | 1) → (2 | 0) side crossing of (1 | 1) at $T \geqslant 52$ K (point (4)) and the short $\lesssim 5$ psec lifetime of the (1 | 1) structure originating from the (2 | 0) → (1 | 1) side crossing (point 6(d)). Despite the energetic stability of the (1 | 1) structure (point (7)) the prevalence of (2 | 0) is due to entropy contributions.

(11) The structural fluctuation parameters are systematically higher for the $(2 \mid 0)$ isomer than for the $(1 \mid 1)$ isomer over the entire temperature coexistence domain (Fig. 1). The high values of the structural fluctuation parameters, e.g. $\sigma > 0.1$ at $T > 10$ K, for the $(2 \mid 0)$ isomer (Fig. 1), reflect the nonrigidity of this structure. Accordingly, the onset of the nonrigid $(2 \mid 0)$ structure of benzene·Ar_2 is specified by $\sigma \geqslant 0.1$, being obtained at $T \geqslant 10$ K, in accord with the nonrigidity criterion, Eq. (5). In contrast, for the $(1 \mid 1)$ benzene·Ar_2 we find that $\sigma < 0.1$ and the structure is rigid over the entire temperature existence range of this isomer.

6 Epilogue

The analysis of the nuclear motion of the benzene·Ar_2 vdW heteroclusters reveals a rich dynamic behavior. The central result pertains to the occurrence of hierarchical isomerization in the "small" benzene·Ar_2 $(2 \mid 0)$ heteroclusters, this providing a qualification of the nature of nonrigidity in large molecular vdW heteroclusters.

The interrelationship between thermodynamic and dynamic size effects in $M \cdot A_n$ heteroclusters is of intrinsic interest. Various isomerization processes were identified by MD and Monte-Carlo computer simulations [16, 17, 31–34]. These involve correlated surface motion (of A atoms on one side of M), surface melting (i.e., uncorrelated motion of A atoms on the microsurface of M), side crossing (of A atoms from one microsurface of A to the other), wetting-nonwetting (or two-dimensional (2D) to three-dimensional (3D)) transition and a rigid-nonrigid transition. Recent studies [16, 32, 33] established the hierarchical occurrence of several isomerization processes for a single heterocluster composition and the sequential occurrence of distinct isomerization processes with increasing the size of the $M \cdot A_n$ heterocluster for a given M. This isomerization pattern is specified by the finite surface density $\varrho_s = n/(\text{M microsurface area})$ of the rare-gas atoms [32]. Benzene·Ar_n heteroclusters, which are characterized by a large value of ϱ_s, were demonstrated to exhibit a hierarchy of isomerization processes even for a small value of $n = 2$. The present analysis demonstrates that the smallest heterocluster of the $M \cdot A_n$ family (as far as the size of the aromatic molecule and the coordination number are concerned), which exhibits distinct isomers, reveals a proliferation of isomerization processes. This state of affairs bears a close analogy to the isomerization of small neat rare-gas clusters, where Ar_3 exhibits a rigid $\rightarrow$ nonrigid transition [35]. The dynamic behavior of these van der Waals molecules (clusters) at finite temperatures marks the breakdown of the traditional description of molecular structure.

References

1. Berry RS (1960) Rev Mod Phys 32:447
2. Wooley RG (1976) Adv Phys 25:27
3. Rosen N, Morse PM (1932) Phys Rev 42:10
4. Dennison DM, Uhlenbeck GE (1932) Phys Rev 41:313
5. Kilpatrick JE, Pitzer KS, Spitzer R (1947) J Am Chem Soc 69:2483
6. Gutowsky HS, McCall DW, Slichter CP (1956) J Chem Phys 21:279
7. Doering W, Roth WR (1956) Angew Chem Intern Engl 2:279

8. Teller E, Wheeler JA (1938) Phys Rev 53:778
9. Martin RL, Davidson ER (1978) Mol Phys 35:1713
10. Bartell LS, Gavin RM (1968) J Chem Phys 48:2466
11. Cotton FA, (1975) J Organomet Chem 100:29
12. Beswick JA, Jortner J (1981) Adv Chem Phys 47:363
13. Amirav A, Even U, Jortner J (1981) J Chem Phys 75:2489
14. Even U, Amirav A, Leutwyler S, Ondrechen MO, Berkovitch-Yellin Z, Jortner J (1982) Faraday Discuss Chem Soc 73:153
15. Leutwyler S, Jortner J (1987) J Phys Chem 91:5558
16. Leutwyler S, Bösiger J (1990) Chem Rev 90:489
17. Leutwyler S, Bösiger J (1987) in: Jortner J, Pullman B, Pullman A (eds) Large finite systems. Reidel, Dordrecht, p 153
18. Kellman ME, Amar F, Berry RS (1979) J Chem Phys 73:2387
19. Kaelberer JB, Etters RD (1977) J Chem Phys 66:3233
20. Couchman PR, Ryan CL (1978) Phil Mag A37:369
21. Schmidt M, Mons M, Le Calvé J (1991) Chem Phys Lett 177:371
22. Schmidt M, Mons M, Le Calvé J, Millié P, Cossart-Magos C (1991) Chem Phys Lett 183:69
23. Ben-Horin N, Even U, Jortner J (1992) Chem Phys Lett 188:73
24. Karplus M (1987) in: Kilmister CW (ed) Schrödinger, Century celebration of a polymath. Cambridge Univ Press, p 85
25. Feynman RP, Hibbs AR (1965) Quantum mechanics and path integrals. McGraw-Hill, NY
26. Scharf D, Landman U, Jortner J (1988) J Chem Phys 88:4273
27. Ondrechen MJ, Berkovitch-Yellin Z, Jortner J (1981) J Am Chem Soc 103:7686
28. Dewar MJS, Thiel W (1977) J Am Chem Soc 99:4899
29. Löwdin PO (1950) J Chem Phys 18:365
30. Stout Jr EQ, Politzer P (1968) Theor Chim Acta 12:379
31. Bösiger J, Knochenmuss R, Leutwyler S (1989) Phys. Rev. Lett. 62:3058
32. Ben-Horin N, Even U, Jortner J, Spectroscopic interrogation of heterocluster isomerization, J Chem Phys (in press)
33. Ben-Horin N, Even U, Jortner J, Leutwyler S, Spectroscopy and nuclear dynamics of tetracene-rare-gas heteroclusters, J Chem Phys (in press)
34. Fried LE, Mukamel S (1991) Phys Rev Lett 66:2340
35. Berry RS, Beck TL, Davis HL, Jellinek J (1988) Adv Chem Phys 70:74